Orbital orientation mapping of V_2O_5 thin films

B. R. Lamoureux, V. Jovic, V. R. Singh, and K. E. Smith

Citation: Journal of Applied Physics **122**, 045305 (2017); doi: 10.1063/1.4993912
View online: http://dx.doi.org/10.1063/1.4993912
View Table of Contents: http://aip.scitation.org/toc/jap/122/4
Published by the American Institute of Physics

Articles you may be interested in

Elevated transition temperature in Ge doped VO_2 thin films
Journal of Applied Physics **122**, 045304 (2017); 10.1063/1.4995965

A comprehensive review of ZnO materials and devices
Journal of Applied Physics **98**, 041301 (2005); 10.1063/1.1992666

Electrochemical characterization of GaN surface states
Journal of Applied Physics **122**, 045302 (2017); 10.1063/1.4995429

The stabilization of the rocksalt structured tantalum nitride
Journal of Applied Physics **122**, 045109 (2017); 10.1063/1.4989415

Periodic arrays of flux-closure domains in ferroelectric thin films with oxide electrodes
Applied Physics Letters **111**, 052901 (2017); 10.1063/1.4996232

Measurement of contact resistivity at metal-tin sulfide (SnS) interfaces
Journal of Applied Physics **122**, 045303 (2017); 10.1063/1.4992086

AIP | Journal of Applied Physics
Save your money for your research.
It's now FREE to publish with us -
no page, color or publication charges apply.
Publish your research in the
Journal of Applied Physics
to claim your place in applied
physics history.

Orbital orientation mapping of V_2O_5 thin films

B. R. Lamoureux,[1] V. Jovic,[2,3] V. R. Singh,[1,4] and K. E. Smith[1,2,3]
[1]*Department of Physics, Boston University, Boston, Massachusetts 02215, USA*
[2]*School of Chemical Sciences, The University of Auckland, Auckland 92019, New Zealand*
[3]*The MacDiarmid Institute for Advanced Materials and Nanotechnology, Victoria University of Wellington, Wellington 6140, New Zealand*
[4]*Department of Physics, Central University of Kashmir, Sonwar, Srinagar 190004, India*

(Received 23 February 2017; accepted 1 July 2017; published online 31 July 2017)

We report the effects of growth methods on the orbital orientation in vanadium pentoxide (V_2O_5) thin films, an important factor to consider when selecting growth techniques for highly selective catalysts and devices. Thermal evaporation and sol-gel methods were used to synthesize the V_2O_5 films. The surface morphology, roughness, and orientation of the films were characterized by atomic force microscopy and x-ray diffraction. Surface electronic properties and oxidation states were assessed by x-ray photoemission spectroscopy. Polarized x-ray absorption spectroscopy demonstrated that the thermally evaporated film [which was in the (001) orientation] exhibited greater anisotropy than the (100) oriented sol-gel film. The observed increase in anisotropy agrees well with computational findings which revealed that more vanadyl bonds are present at the surface of the thermally evaporated film than at the surface of the sol-gel film. The same computational study also found that the orientation of these bonds is more parallel to the film surface in the thermally evaporated film than in the sol-gel film. The data suggest that the method of growth may be used as a controlled variable to select key film characteristics for potential applications. *Published by AIP Publishing.* [http://dx.doi.org/10.1063/1.4993912]

INTRODUCTION

Vanadium pentoxide (V_2O_5) exhibits diverse electronic and magnetic properties, which make this material a promising platform for the development of nanoscale, multifunctional electronic, spintronic devices, and coatings on smart windows.[1–5] V_2O_5 has also gained attention as a potential material for increased green energy storage in capacitors.[6] As a catalyst, V_2O_5 has been used in reactions ranging from transesterification to the oxidative coupling of 2-napthol.[7,8] V_2O_5 thin film catalysis supported on a highly ordered metal oxide has been a popular choice due to its low cost, allowing for tunable reactant selectivity, fixed orbital orientation, and mass transfer limitations through substrate choice.[7,9–11] V_2O_5 photocatalysts have also proven to be effective in the degradation of water pollutants and are used in the oxidative dehydrogenation of propane to obtain hydrogen gas and propylene on an industrial scale.[8,12]

To facilitate the rational design and performance optimization of devices and catalysts, it is important to understand the effect of the film orientation on the electronic structure. Polarized x-ray absorption spectroscopy (XAS) is one of the most powerful tools available for studying the orbital orientation within epitaxial films. Features observed along the $L_{3,2}$-edge of transition metal oxides were not successfully accounted for until foundational computational studies incorporated crystal field effects through the employment of atomic multiplet models.[13,14] Although a correlation between observed transitions and molecular orbitals in V_2O_5 has been made, this knowledge has not been applied to study the effect of synthesis techniques on the orbital orientation of thin films. This is an important factor to consider when choosing a technique for efficiently fabricating highly selective catalysts and devices.[15,16]

In this study, we describe the synthesis and characterization of epitaxial V_2O_5 thin films grown on *c*-plane sapphire by both thermal evaporation and sol-gel methods. The orientation and morphology of the films are probed by x-ray diffraction (XRD) and atomic force microscopy (AFM), respectively. The oxidation states in the near surface region of the films are assessed by x-ray photoemission spectroscopy (XPS). Finally, polarized XAS is used to probe the orbital orientation in the films. Collectively, this suite of physicochemical characterization techniques provides insights into the effects of growth methods on the orbital orientation.

EXPERIMENTAL

Thermal evaporation

V_2O_5 powder (>99.6%) was deposited from a tantalum boat onto a *c*-plane (0001) sapphire substrate. The boat was kept as far away from the substrate as possible (12.7 ± 0.5 cm) to limit substrate heating during the growth process. The film was grown in a vacuum chamber with a base pressure of $\sim 1 \times 10^{-7}$ Torr. Prior to growth, the substrate surface was cleaned by rinsing with deionized water, then dipping in H_2O_2:NaOH:H_2O in the ratio of 1:1:100, and finally sonicating the substrate in ethanol. The substrate was then dried with a stream of room temperature N_2 gas. Film growth was achieved by passing a current of 35 A through a tungsten filament (wrapped around the tantalum boat) for 30 min.

Sol-gel

For the sol-gel film, 2-propanol, acetyl acetone, and vanadium oxytriisopropoxide in a molar ratio of 1:1:20 were vigorously stirred for 2 h in a sealed container. Exposure to

air allowed nanocrystals to form and precipitate out of the solution. To limit air exposure, the solution was immediately spin coated onto a *c*-plane (0001) sapphire substrate which was pre-cleaned and dried in the same manner as was mentioned for the thermally evaporated film.[17] Both films were annealed under high oxygen pressure [10 standard liters per minute (SPLM)] for 30 min at 500 °C.

XRD patterns of the V_2O_5 thin films were collected on a Bruker D8 high resolution x-ray diffractometer. Radiation from a Cu K_α source ($\lambda = 1.5418$ Å) was refined by a Gobel mirror to filter out Cu K_β radiation and two 0.2 mm width slits: one positioned directly in front of the sample and the other directly prior to the lynxe eye detector. The system was operated at 45 kV and 40 mA with an angular resolution of 0.001° across a 2θ range of 15°–65°. The surface morphology of the thin films was also examined using a Digital Instruments AFM. AFM analysis on the V_2O_5 thin films was performed in the tapping mode.

XPS data were collected using a Scienta hemispherical electron energy analyzer with monochromatic x-rays generated by an aluminum K_α anode. The base pressure of the vacuum chamber was 1.8×10^{-9} Torr during measurements. The spectra were calibrated with respect to a gold reference foil. XAS measurements were performed at beamline 8.0.1 at the Advanced Light Source, Lawrence Berkeley National Laboratory. Data were collected in the bulk sensitive total fluorescence yield (TFY) mode, with a probing depth of ~100 nm. The energy scales of XAS spectra at the V *L*- and O *K*-edges were calibrated with reference to the Ti *L*- and O *K*-edge XAS spectra of rutile TiO_2. Spectral resolution for the measurements was approximately 0.2 eV at full width at half maximum (FWHM). The photon flux was 2.2×10^{12} photons s^{-1}. Pressures in the analysis chamber were maintained below 10^{-9} Torr during XAS measurements. All measurements were undertaken at room temperature. A Savitzky-Golay filter was applied to filter out undesirable noise from the spectra.

RESULTS AND DISCUSSION

Figure 1(a) displays XRD patterns for epitaxial V_2O_5 thin films deposited onto *c*-plane sapphire substrates by the thermal evaporation method (shown in blue) and sol-gel method (shown in black). Furthermore, this plot also shows an XRD pattern from a pure *c*-plane sapphire substrate (shown in red). Substrate peaks in the XRD patterns of the sol-gel and thermally evaporated films are marked by an asterisk. By matching experimental diffraction patterns to the V_2O_5 pattern in the JCPDS database (#00-041-1426, 1991)[18] and with previous studies,[19,20] we find that the sol-gel film is oriented in the (100) direction (with characteristic peaks at $2\theta = 31.05°$ and $2\theta = 47.33°$) and that the thermally evaporated film is oriented in the (001) direction (with a characteristic peak at 24.40°). Additional substrate peaks in the XRD pattern of the sol-gel film arise from residual Cu K_β radiation that was not filtered out by the Gobel mirror. In previous studies, it has been shown that techniques which involve heat during deposition (i.e., chemical vapor deposition and pulsed laser deposition) yield an epitaxial (001)

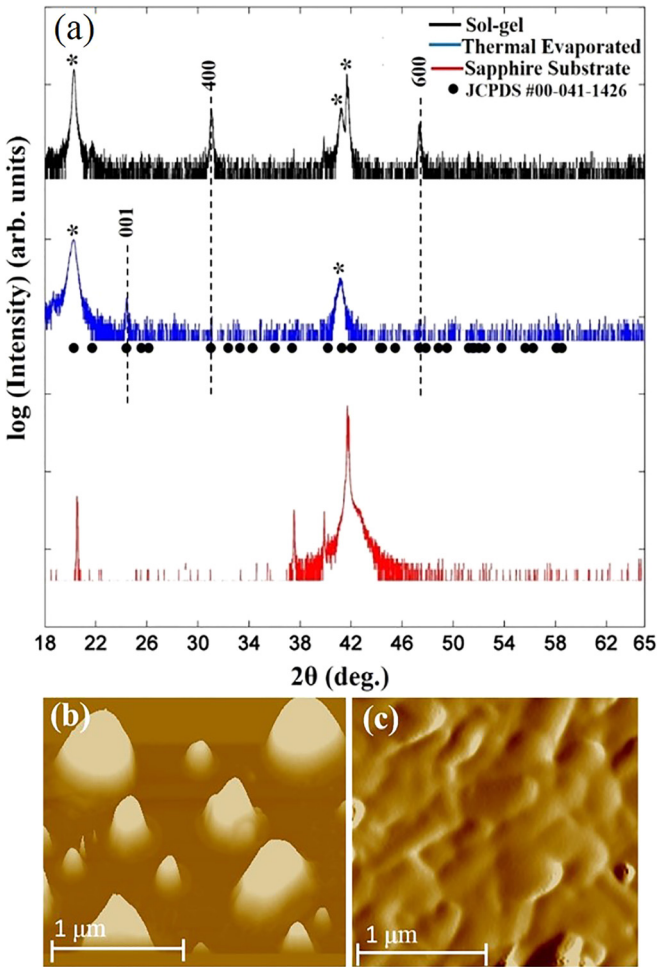

FIG. 1. Panel (a) presents the XRD patterns for V_2O_5 epitaxial films grown by the sol-gel method (shown in black) and the thermal evaporation method (shown in blue). JCPDS reference data of a V_2O_5 powder (#00-041-1426, 1991) is also shown by the black dots. A sapphire substrate (shown in red) is also included for comparison. Points marked by the stars correspond to substrate peaks in the V_2O_5 XRD patterns. Panel (b) shows an AFM image of the thermally evaporated film. Panel (c) shows an AFM image of the sol-gel film. AFM analysis was performed in the tapping mode.

V_2O_5 film, whereas room temperature deposition techniques (i.e., sol-gel) yield highly ordered films where either (100) or (001) is nearly equal in the concentration or (100) is the dominant orientation.[1,21–23] Our own results fit the trend observed in the literature and show that indeed the use of a technique involving heat favored a (001) orientation while the room temperature technique allowed the (100) orientation to persist. We suggest that the thermally evaporated and sol-gel films have different orientations, despite being grown on the same substrate, for two reasons; (i) hot techniques allow V_2O_5 to settle into the most thermodynamically favorable state, while, during spin coating, deposited V_2O_5 is in a pseudo solvated state and remains in this kinetically driven state even after the solvent has evaporated off; and (ii) the sapphire substrate is hexagonal, meaning that crystal axes *a* and *b* are equal. This presents a larger number of strain minimizing configurations available for the deposited V_2O_5.[24]

AFM imaging shows the surface morphology of the thermally evaporated film [Fig. 1(b)] and sol-gel film [Fig. 1(c)]. The root mean square roughness was found to be

12 nm and 106 nm for the sol-gel and thermally evaporated films, respectively. We note from a previous study that thermally evaporated films grown under the same conditions as the one presented here, but which received no post-growth annealing, did not show clustering and had a surface roughness of ∼1.5 Å.[17] The contrasting images and roughness between thermally evaporated films that were annealed and those that were not suggest that clustering occurred as the film cooled following annealing at the higher temperature. Previously, we determined that thermally evaporated films grown under the same conditions had a thickness of ∼50 nm (Ref. 17), and the sol-gel film was determined to be ∼80 nm.[16] XPS spectra (Fig. 2) of both the sol-gel and thermally evaporated films have the characteristic V $2p_{3/2}$ peak at 516.5 ± 0.1 eV and 516.6 ± 0.1 eV, respectively, and an O 1*s* feature at 529.8 ± 0.1 eV. The binding energies are consistent with vanadium in the 5+ oxidation state in V_2O_5.[25]

The XAS V *L*-edge spectrum for the sol-gel film recorded in total fluorescence yield (TFY) is presented in Fig. 3. X-ray absorption at the V *L*-edge corresponds to transitions from the V 2*p* core levels to unoccupied V 3*d* orbitals. The L_2 and L_3 doublets originate from spin-orbit splitting of the V 2*p* core levels into V $2p_{1/2}$ and V $2p_{3/2}$. The fine structure along the L_3-edge arises from the crystal field splitting of the V 3*d* orbitals. Although there should be an equal number of features along the L_2 and L_3 edges, the fine structure along the L_2-edge is masked by life-time broadening arising from a Coster-Kronig decay channel into the $2p_{3/2}$ core hole.[15,26] In the work by Goering *et al.*, the spectral features along the L_3-edge of V_2O_5 were originally labeled as V_1-V_7 at 515.9 eV, 517.1 eV, 517.6 eV, 518.2 eV, 518.8 eV, 519.4 eV, and 515.2 eV, respectively.[15] Throughout this work, we use the labeling system introduced by Goering *et al.* By comparing V 3*d* partial DOS calculations[14] and the features observed in their experimental

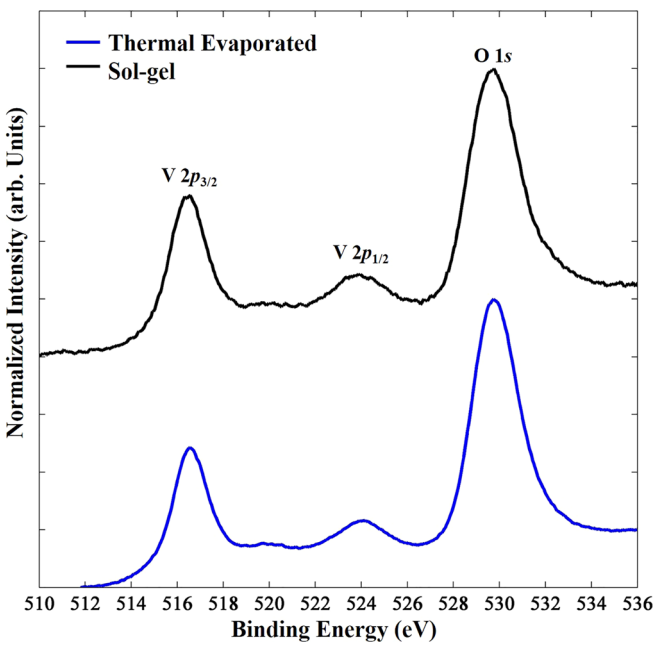

FIG. 2. XPS spectra for V_2O_5 grown by the thermal evaporation (shown in blue) and sol-gel (shown in black) methods. The films were grown on a *c*-sapphire substrate. Spectra were recorded at room temperature.

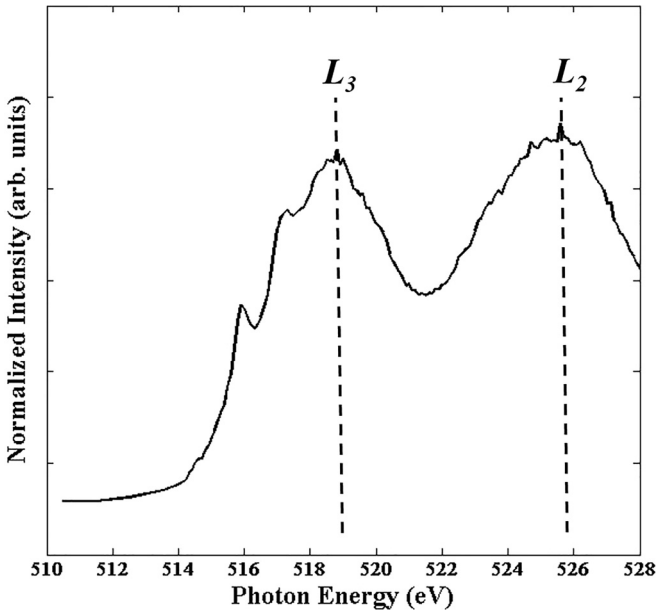

FIG. 3. Vanadium *L*-edge XAS spectrum of V_2O_5 grown using the sol-gel method on *c*-plane sapphire. The spectrum was collected at room temperature in the TFY mode. A distinct doublet can be seen, which corresponds to the L_3- and L_2-edges, with a clear fine structure present along the L_3-edge.

angular dependent XAS measurements,[15] it becomes clear that the lower energy features, V_1-V_3 and V_7, can be associated with the t_{2g} molecular orbitals, whereas the higher energy peaks, V_4-V_6, are associated with the e_g molecular orbitals.[15]

Generally, peak intensities in XAS spectra are proportional to the number of unoccupied states with the specific symmetry and orientation for a dipole transition from the original core level. Three main factors contribute to the strong anisotropic XAS spectra observed in V_2O_5. First, the layered structure is fundamentally highly anisotropic. Its lattice also has a two-dimensional character, which reduces dispersion effects, ultimately resulting in sharp absorption features.[14] Finally, before excitation, it is initially in a $3d^0$ system, which largely reduces final-state splitting through the *d*-*d* Coulombic interactions.[15] Throughout the polarization dependent x-ray absorption measurements performed in this study, the relative geometries are as follows: (i) in-plane—which corresponds to $E_{||a}$ for the (100) sol-gel film and $E_{||c}$ for the (001) thermally evaporated film and (ii) out-of-plane—corresponding to $E_{||bc}$ for the sol-gel film and $E_{||ab}$ for the thermally evaporated film. A diagram showing the geometric orientation of the incident light and the crystal axis for each film can be found in Fig. 1 in the supplementary material.

Figure 4 presents the XAS spectra of the sol-gel film, recorded in the TFY mode, for both the $E_{||a}$ (shown in red) and the $E_{||bc}$ (shown in black) orientations. For $E_{||a}$, the spectrum shows a very smooth, broad V_4 peak and a small peak at the V_1 position. When the orientation is changed from $E_{||a}$ to $E_{||bc}$, the V_1 feature becomes more distinct and the V_4 peak splits into the V_3 and V_5 features. The development of the V_3 feature, which is associated with the t_{2g} molecular orbital, is a direct consequence of increased coupling between the orbital wavefunctions of the d_{xy}, d_{xz}, d_{yz}, and the incident light. The observation suggests that these orbitals lie more along the

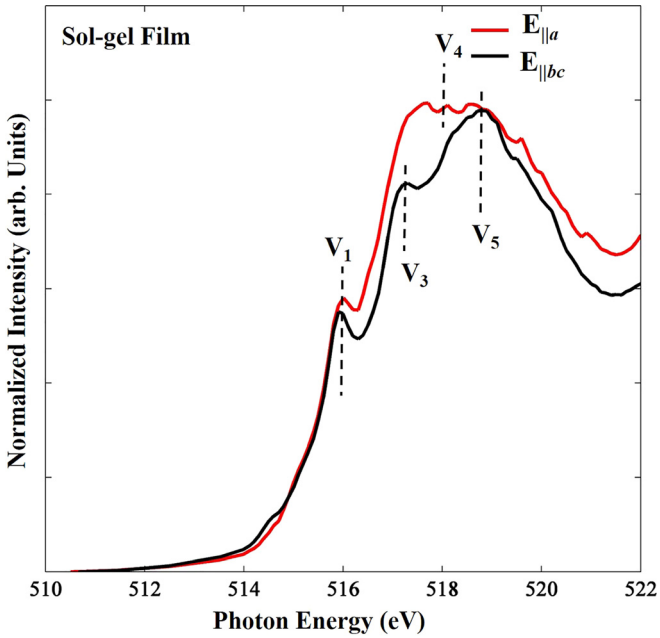

FIG. 4. Polarization dependent XAS measurements at the L_3-ege of the (100) V_2O_5 film grown by the sol-gel method. The spectrum was collected at room temperature in the TFY mode.

bc-plane than the *a*-axis. In a series of computational calculations focused on the band structure of V_2O_5, distortions where the vanadyl oxygen and vanadium atoms have a slight vertical displacement resulted in a broadening of the V d_{xy} d_{yz}, and $d_{x^2-y^2}$ orbitals.[14] Because these orbitals are involved in the allowed transitions from V 2*p* states, it is possible that the observed broadening at the L_3-edge is a result of these distortions.

The XAS spectra from the thermally evaporated film taken in the TFY mode are presented in Fig. 5. In the $E_{||c}$

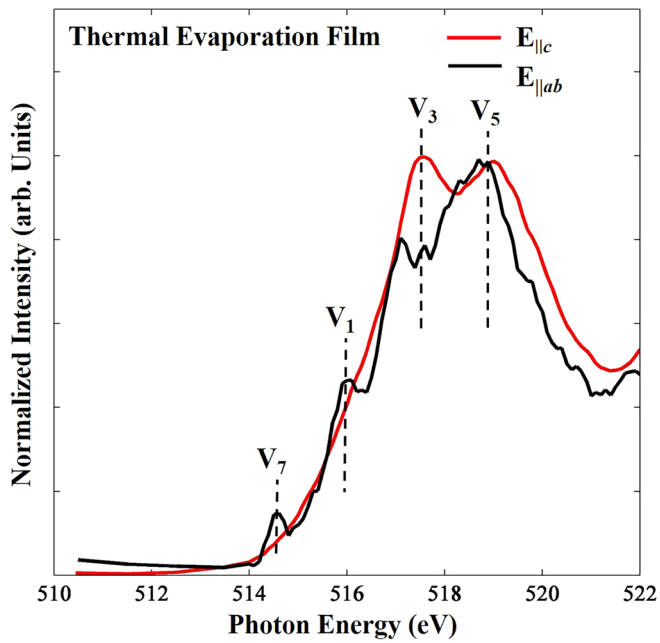

FIG. 5. Polarization dependent XAS measurements at the L_3-ege of the (001) V_2O_5 film grown by the thermal evaporation method. As for the sol-gel film, spectra were collected at room temperature in the TFY mode.

measurement orientation, there is a strong doublet on the L_3-edge, which is consistent with the V_3 and V_5 features. In the $E_{||ab}$ orientation, there is a distinct increase in the splitting of the V_3 and V_5 features, and the V_1 and V_7 features emerge. The observed increase in the peaks associated with the t_{2g} molecular orbital (the V_1, V_3, and V_7) in the $E_{||ab}$ probing orientation indicates, just as with the $E_{||bc}$ orientation of the sol-gel film, that there is a more direct probing of these orbitals by the incident light. This suggests that the t_{2g} molecular orbitals lie more along the *ab*-plane than the *c*-axis. It should be noted that there is a shift of the V_7 peak down to lower energy (~0.9 eV) in the $E_{||ab}$ orientation when compared to the results reported by Goering *et al.*[15] In a similar fashion to the sol-gel film, where the breadth of V_4 can be explained by the vertical displacement of the vanadyl oxygen and the vanadium atoms, the drift in the lowest lying t_{2g} orbital (V_7 peak) might arise from the same distortions.[14]

Although the two films have different orientations, both present similar features in the XAS spectra, suggesting that the two films have a similar surface bond character. Recently, computational diagrams of V_2O_5 for different miller indices reported that both the (100) and (001) orientations, which correspond to the sol-gel and thermally evaporated films, respectively, have vanadyl bonds at the surface of the film.[28] The consistency between the computational findings and experimental observation provides good evidence that the surface bonding character is similar for the two films.

While the V *L*-edge provides information about the *d* orbitals within the conduction band, XAS at the O *K*-edge involves electronic transitions from the O 1*s* to O 2*p* states that are hybridized with V t_{2g}* and V e_g* molecular orbitals.[16] The two main features along this edge are ascribed to the π^* (~529.6 eV) and σ^* (~531.3 eV) orbitals (Fig. 6). In both films, there is a significant shift in the spectral weight from the σ^* into the π^* orbital as the incident light transitions from $E_{||a} \rightarrow E_{||bc}$ and $E_{||c} \rightarrow E_{||ab}$ for the sol-gel and thermally evaporated film, respectively. Although there is a pronounced anisotropy observed in both films, the thermally evaporated film presents a larger shift than the sol-gel film. The evolution of the σ^* peak, which is associated with the vanadyl bond,[27] suggests that there is a more direct probing of these bonds within the thermally evaporated film. Again, this observation supports computational calculations which demonstrated that vanadyl bonds in films of the (100) orientation (that of the sol-gel film) are more perpendicular to the film surface than films oriented in the (001) direction (as in the thermally evaporated film).[28]

Overall, the two films show significant anisotropy in the peaks associated with the t_{2g} molecular orbitals (the V_1-V_3 and V_7) along the V *L*-edge and the π^* and σ^* along the O *K*-edge. This similarity in features present in both spectra is consistent with computational results, performed by Sayle *et al.*, which showed that the vanadyl bond protrudes from the film surface for both the (100) and (001) orientations of V_2O_5.[28] While both films did show anisotropy, there was significantly more anisotropy along both the V *L*-edge and O *K*-edge for the thermally evaporated film. When the increased anisotropy in the (001) thermally evaporated film is taken in context with band structure calculations, it becomes clear

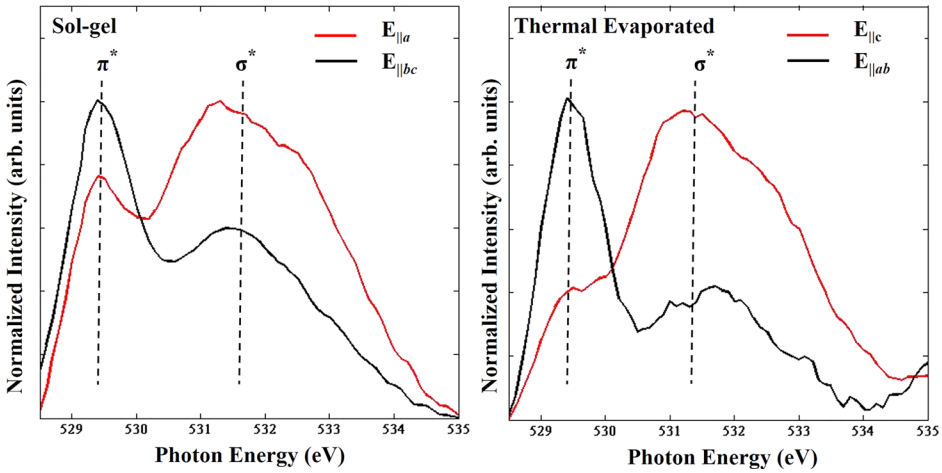

FIG. 6. (Left) Polarization dependent XAS measurements at the O *K*-edge of the (100) V_2O_5 sol-gel grown film. (Right) Polarization dependent XAS measurements at the O *K*-edge of the (001) V_2O_5 thermal evaporation grown film. Spectra for both films were collected at room temperature in the TFY mode. Stronger coupling to π^*, in both films, for the out-of-plane orientation can be seen.

that there is a more direct probing of the t_{2g} molecular orbitals in the (001) orientation when compared to films oriented in the (100) direction. The stronger coupling to the t_{2g} molecular orbitals in the $E_{||ab}$ probing geometry for the thermally evaporated film in comparison to the $E_{||bc}$ probing geometry for the sol-gel film is also consistent with the finding, from Sayle *et al.*, that the vanadyl bonds in the (100) orientation are more normal to the film surface than the vanadyl bonds of films in the (001) orientation.[28] The ability to select the orientation and character of bonds that protrude from a films surface suggests that the growth method could be used as a controlled variable to select the surface orbital orientation most appropriate for a desired application. In the future, determining the catalytic efficiency of each film could further evaluate the success of using the synthesis technique as a method for fine tuning the surface orbital orientation. Furthermore, experiments which vary the growth substrate would be beneficial in determining if the protrusion of the vandyl bond is structurally or electronically driven.

CONCLUSION

In this study, epitaxial V_2O_5 films grown by the sol-gel and thermal evaporation methods were electronically and structurally characterized by XRD, AFM, XPS, and XAS. XRD patterns verified that the sol-gel film had a (100) orientation and the thermally evaporated film had a (001) orientation. Electronically, both films presented the V $2p_{3/2}$ and O 1*s* XPS peaks at energies consistent with V_2O_5 (i.e., vanadium being in the 5+ oxidation state). Polarization dependent XAS measurements along the V *L*-edge showed that peaks related to the t_{2g} molecular orbitals were more collinear than perpendicular with the principal axis for both films. Furthermore, through polarization dependent XAS along the O *K*-edge, it was observed that both films showed a shift in the spectral weight from the σ^* into the π^* orbital as the incident light transitioned from probing parallel to the principle axis to perpendicular with it. The similar electronic character for both films along the V *L*- and O *K*-edges supports computational findings that the vanadyl bond is the prominent bond at the surface of the film for both the (001) and (100) orientations. In addition, a larger anisotropy was observed along both the V *L*- and O *K*-edges in the thermally evaporated film as compared to the sol-gel film. This is consistent with computational findings which showed that the vanadyl bond is slightly more collinear with the principal axis in the sol-gel film than in the thermally evaporated film. Overall, it was shown that the surface orbital orientation is influenced by the growth method. This suggests that the growth method may be used as a controlled variable to select the surface orbital orientation most appropriate for a desired application.

SUPPLEMENTARY MATERIAL

See supplementary material for the propagation of light relative to the crystal axes of the sol-gel and thermally evaporated sample are clearly indicated in Fig. 1.

ACKNOWLEDGMENTS

We would like to thank Dr. Wanli Yang, Jeffery Bacon, Elbara Ziade, and Ruimin Qiao for their technical help and support. This research was performed in part in the Central Facilities of the Boston University, which was supported by the Boston Research Initiative. The Boston University program was supported by the Department of Energy under Grant No. DE-FG02-98ER45680. The Advanced Light Source was supported by the U.S. Department of Energy under Contract No. DE-AC02-05CH11231.

[1]J. M. Velazquez, C. Jaye, D. Fischer, and S. Banerjee, J. Phys. Chem. **113**, 7639 (2009).
[2]Y. Fujuita, K. Miyazaki, and C. Tatsuyama, Jpn. J. Appl. Phys., Part 1 **24**, 1082 (1985).
[3]K. Nagase, Y. Shimizu, N. Miura, and N. Yamazoe, Appl. Phys. Lett. **60**, 802 (1992).
[4]O. M. Osmolovskaya, I. V. Murin, V. M. Smirnov, and M. G. Osmolovsky, Rev. Adv. Mater. Sci. **36**, 70 (2014).
[5]Y. Shimizu, K. Nagase, and N. Miura, J. Appl. Phys. **29**, 1709 (1990).
[6]A. Ghosh, E. J. Ra, M. Jin, H.-K. Jeong, T. H. Kim, G. Biswas, and Y. H. Lee, J. Adv. Funct. Mater. **21**, 2541 (2011).
[7]D. Kapolnek, X. H. Wu, B. Heying, S. Keller, B. P. Keller, U. K. Mishra, S. P. DenBaars, and J. S. Speck, Appl. Phys. Lett. **67**, 1541 (1995).
[8]S. Lee, T. Meyer, S. Park, T. Egami, and H. N. Lee, Appl. Phys. Lett. **105**, 223515 (2014).
[9]C. Julien, J. P. Guesdon, A. Gorenstien, A. Khelfa, and I. Ivanov, Appl. Surf. Lett. **90**, 389 (1995).
[10]M. S. de Castro, C. L. Ferreira, and R. R. de Avillez, Infrared Phys. Technol. **60**, 103 (2013).

[11]L. Murawski, C. Gledel, C. Sanchez, J. Livage, and J. P. Audieres, J. Non-Cryst. Solids **89**, 98 (1987).
[12]C. V. Ramana, R. J. Smith, O. M. Hussain, and C. M. Julien, J. Vac. Sci. Tecnol. A **22**, 2453 (2014).
[13]F. M. F. de Groot, J. C. Fuggle, B. T. Thole, and G. A. Sawatzky, Phys. Rev. B **41**, 928 (1990).
[14]V. Eyert and K. H. Hock, J. Phys. Rev. B **57**, 12727 (1998).
[15]E. Goering, O. Muller, M. Klemm, M. L. DenBoer, and S. Horn, Philos. Mag. B **75**, 229 (1997).
[16]B. Chen, J. Laverock, D. Newby, T. Y. Su, K. E. Smith, W. Wu, L. H. Doerrer, N. F. Quackenbush, S. Sallis, L. F. J. Piper, D. A. Fischer, and J. C. Woicik, J. Phys. Chem. C **118**, 1081 (2015).
[17]B. Lamoureux, V. R. Singh, V. Jovic, J. Kuyyalil, T.-Y. Su, and K. E. Smith, Thin Solid Films **615**, 409 (2016).
[18]JCPDS database, PDF -4+ 2014, #00-041-1426, edited by S. Kabekkodu (1991).
[19]Y. Qian, A. Vu, W. Smyrl, and A. Stein, J. Electrochem. Soc. **159**(8), A1135 (2012).
[20]Y. D. Ji, T. S. Pan, Z. Bi, W. Z. Liang, Y. Zhang, H. Z. Zheng, Q. Y. Wen, H. W. Zhang, C. L. Chen, Q. X. Jia, and Y. Lin, Appl. Phys. Lett. **101**, 071902 (2012).
[21]L. Shoa, K. Wu, X. Lin, M. Shui, R. Ma, D. Wang, N. Long, Y. Ren, and J. Shu, Ceram. Int. **40**, 6115 (2014).
[22]P. Viswanathamurthi, N. Bhattarai, H. Y. Kim, and D. R. Lee, Scr. Mater. **49**, 577 (2003).
[23]S. Zhuikov, W. Wlodarski, and Y. Li, Sens. Actuators, B **77**, 484 (2001).
[24]R. Enjalbert and J. Galey, Acta Crystallogr. **42**, 1467 (1986).
[25]J. Mendialdua, R. Casanova, and Y. Barbaux, J. Electron. Spectrosc. Relat. Phenom. **71**, 249 (1995).
[26]J. Zaanen, G. A. Sawatzky, J. Fink, W. Speier, and J. C. Fuggle, Phys. Rev. B **32**, 4905 (1985).
[27]J. Laverock, A. R. H. Preston, B. Chen, J. McNulty, K. E. Smith, L. F. J. Piper, P. A. Glans, J. H. Guo, C. Marin, E. Janod, and V. T. Phuoc, Phys. Rev. B **84**, 155103 (2011).
[28]D. C. Sayle, D. H. Gay, A. L. Rohl, C. R. A. Catlow, J. H. Harding, and M. A. Perrid, J. Mater. Chem. **6**, 653 (1996).